Electronic Supplementary Material (ESI) for Materials Horizons.

Supporting Information: A comprehensive picture of roughness evolution in organic crystalline growth: The role of molecular aspect ratio

Jordan T. Dull,[†,‖] Xiangyu Chen,[‡,‖] Holly M. Johnson,[†] Maria Clara Otani,[†] Frank Schreiber,[¶] Paulette Clancy,[*,‡] and Barry P. Rand[*,†,§]

†*Department of Electrical Engineering, Princeton University, Princeton, NJ 08544, USA*

‡*Department of Chemical and Biomolecular Engineering, Johns Hopkins University, Baltimore, MD 21218, USA*

¶*Institute for Applied Physics, University of Tübingen, 72076 Tübingen, Germany*

§*Andlinger Center for Energy and the Environment, Princeton University, Princeton, NJ 08544, USA*

‖*Contributed equally to this work*

E-mail: pclancy3@jhu.edu; brand@princeton.edu

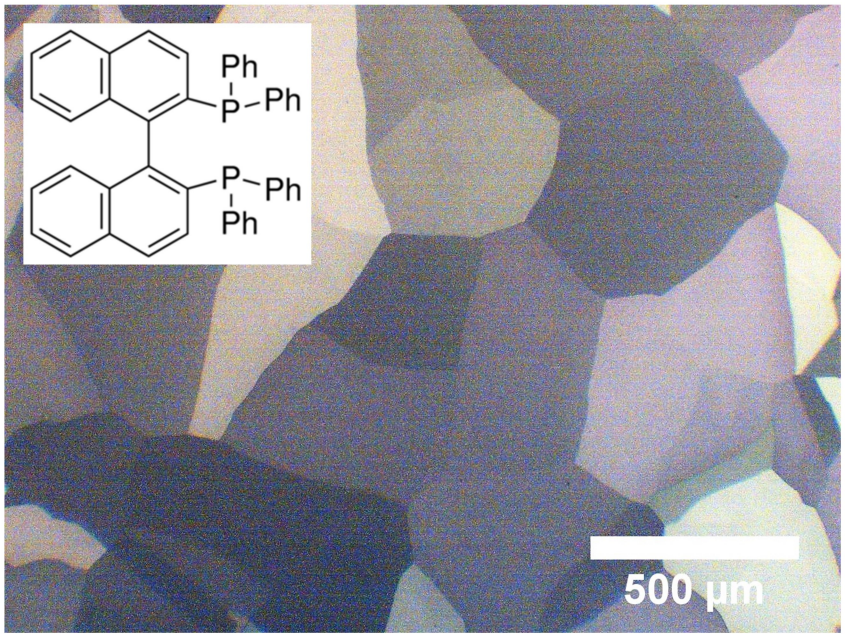

Figure S1: Polarized optical microscope image of a rac-BINAP template layer along with its molecular structure. This film was prepared by depositing 60 nm of rac-BINAP onto a glass/ITO substrate followed by an annealing step on a pre-heated hot plate set to 140 °C for 5 min.

Table S1: Molecules, growth conditions, and results of the roughness evolution experiments.

Molecule	Growth Exponent (β)	Aspect Ratio	Deposition Conditions (Å/s; °C)	Substrate & σ (nm)[a]	Source[b]
C_{60}	-0.04 ± 0.08	1	0.1; 80	NPB; 1.3	tw
TPBi	-0.03 ± 0.07	1.78	0.1; 80	TPBi; 1.1	tw
Rubrene	0.07 ± 0.03	1.80	0.1; 80	Rubrene; 0.8	tw
NPB	0.12 ± 0.06	1.72	0.1; 80	NPB; 1.3	tw
4CzIPN	0.14 ± 0.05	1.55	0.1; ∼100	4CzIPN; 1.1	tw
rac-BINAP	0.16 ± 0.06	1.30	1; 80	rac-BINAP; 0.5	tw
PDI8-CN2	0.27 ± 0.01	3.76	0.03,0.21; 120, 80	Si/SiO_2	1,2
Pentacene	0.57 ± 0.07	4.89	0.1; 80	Si/SiO_2	tw
6P	0.62 ± 0.14	8.44	0.05; RT	mica	3
α-6T	0.58 ± 0.10	7.68	0.1; 80	Si/SiO_2	tw
DIP	0.73 ± 0.03	5.53	0.2; 145	Si/SiO_2	4
H_2Pc	1.03 ± 0.04	4.24	5; RT	glass	5

[a]If an organic molecule is given, then that material's crystalline template was used as the substrate. If given, σ is the RMS roughness of the substrate. [b]tw: this work

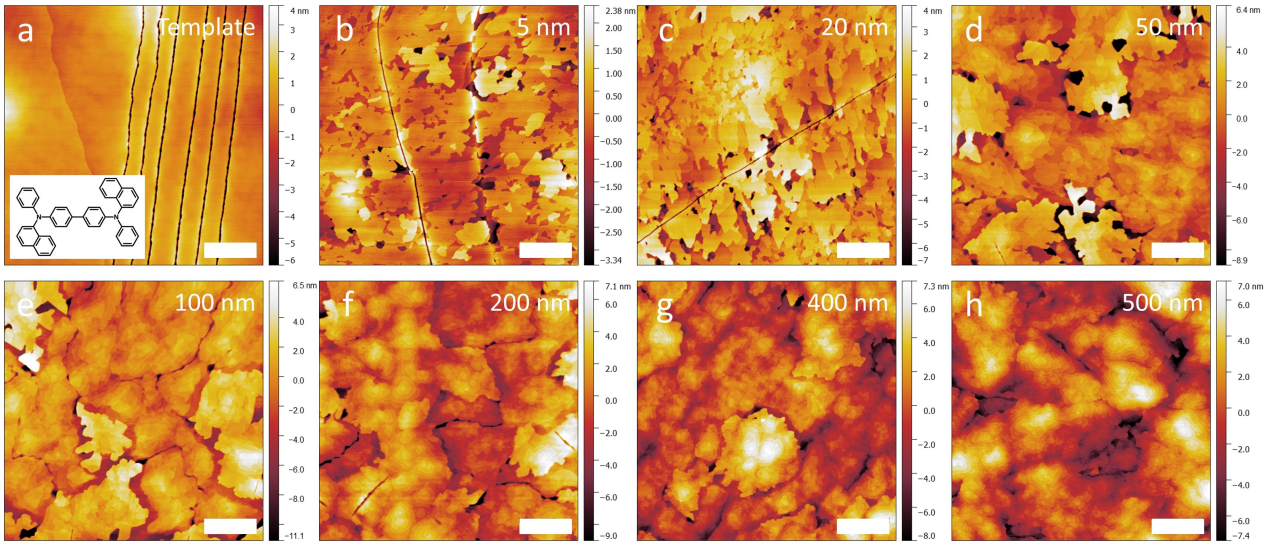

Figure S2: Atomic force microscope scans of NPB deposited at a rate of 0.1 Å/s on a crystalline NPB template layer heated to 80 °C. Adlayer thicknesses are given in the top-right corner of each image. The template layer was prepared as previously reported.[6] Scale bar is 1 μm.

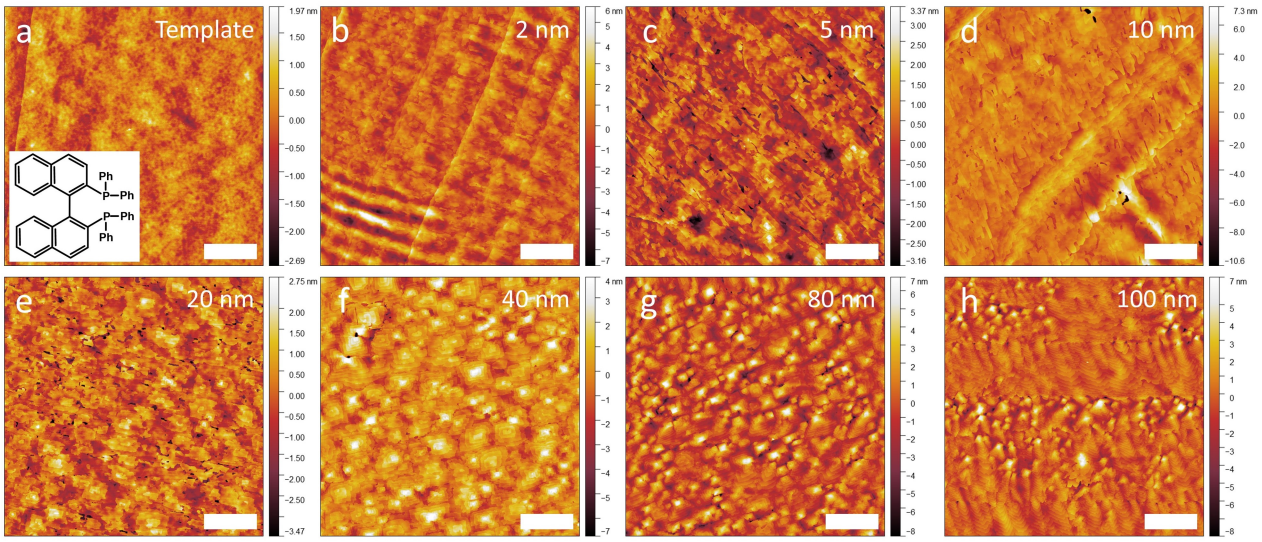

Figure S3: Atomic force microscope scans of rac-BINAP deposited at a rate of 1 Å/s on a crystalline rac-BINAP template layer heated to 80 °C. Adlayer thicknesses are given in the top-right corner of each image. The template layer was prepared by depositing 60 nm of rac-BINAP on a glass/ITO substrate and annealing at 140 °C for 5 min in a nitrogen filled glovebox. Scale bar is 2 μm.

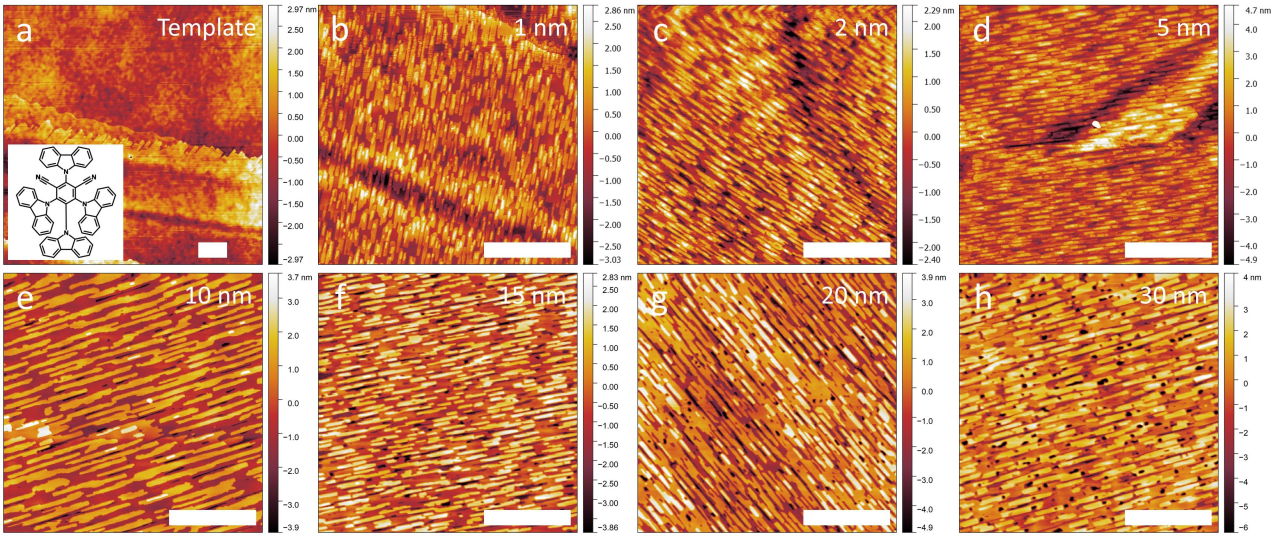

Figure S4: Atomic force microscope scans of 4CzIPN deposited at a rate of 0.1 Å/s on a crystalline 4CzIPN template layer heated to ∼100 °C. Adlayer thicknesses are given in the top-right corner of each image. The template layer was prepared as previously reported.[6] Scale bar is 1 μm.

.

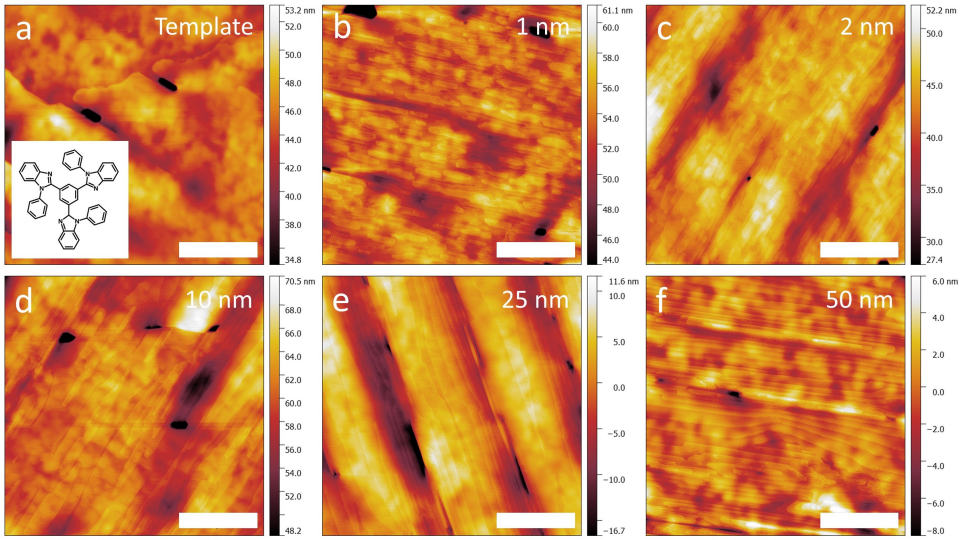

Figure S5: Atomic force microscope scans of TPBi deposited at a rate of 0.1 Å/s on a crystalline TPBi template layer heated to 80 °C. Adlayer thicknesses are given in the top-right corner of each image. The template layer was prepared as previously reported.[6] Scale bar is 3 μm.

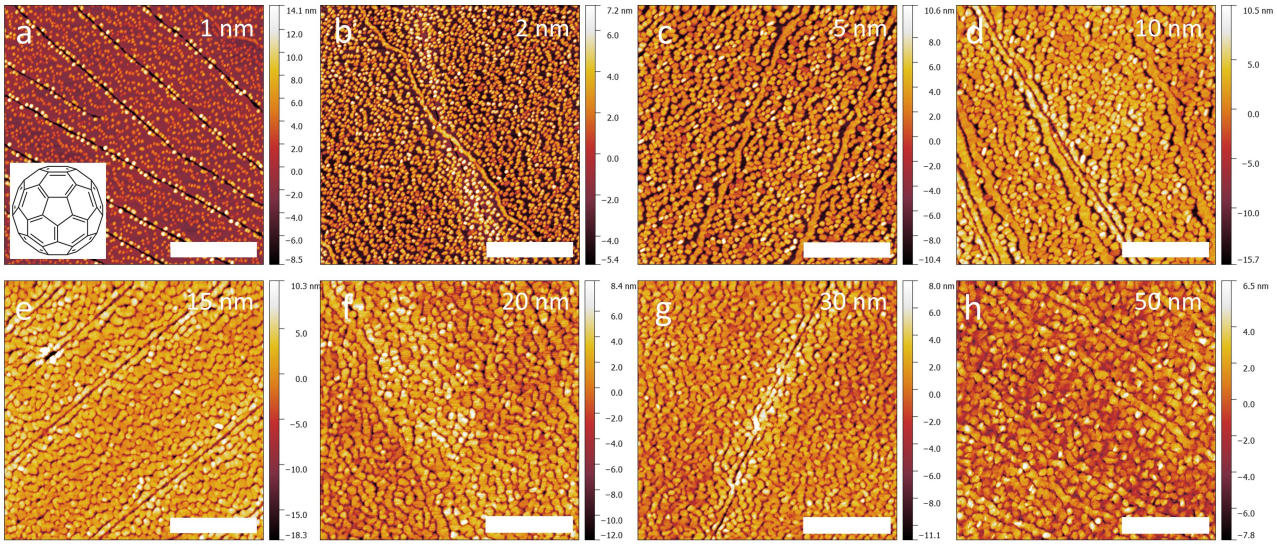

Figure S6: Atomic force microscope scans of C_{60} deposited at a rate of 0.1 Å/s on a crystalline NPB template layer heated to 80 °C. Adlayer thicknesses are given in the top-right corner of each image. The template layer was prepared as previously reported.[6] Scale bar is 1 μm.

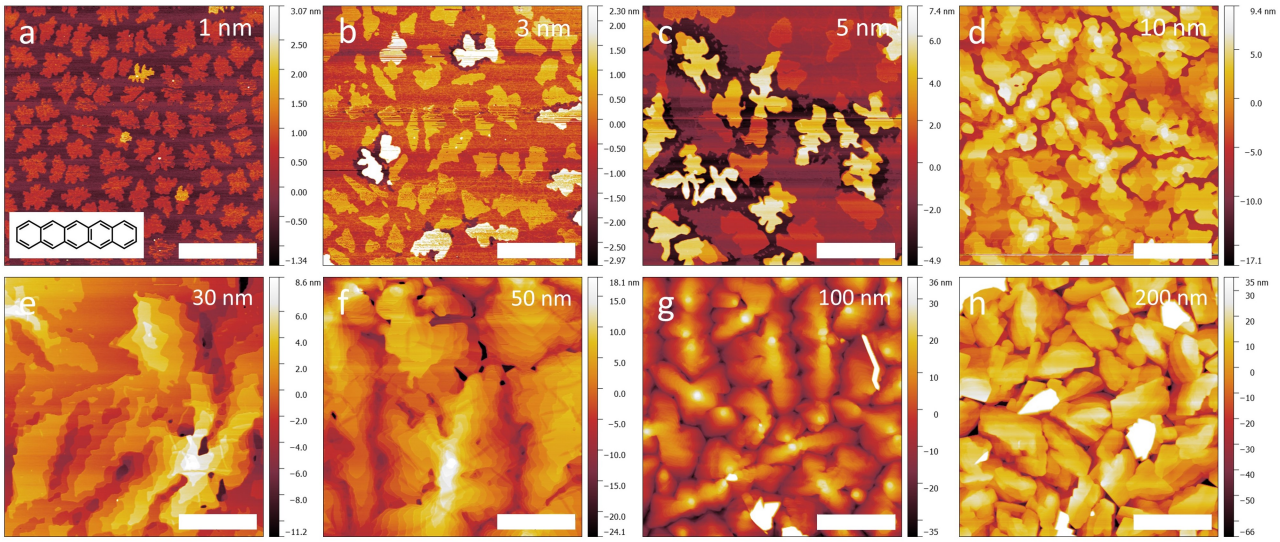

Figure S7: Atomic force microscope scans of pentacene deposited at a rate of 0.1 Å/s on a Si/SiO_2 substrate heated to 80 °C. Layer thickness is given in the top-right corner of each image. Scale bar is 3 μm.

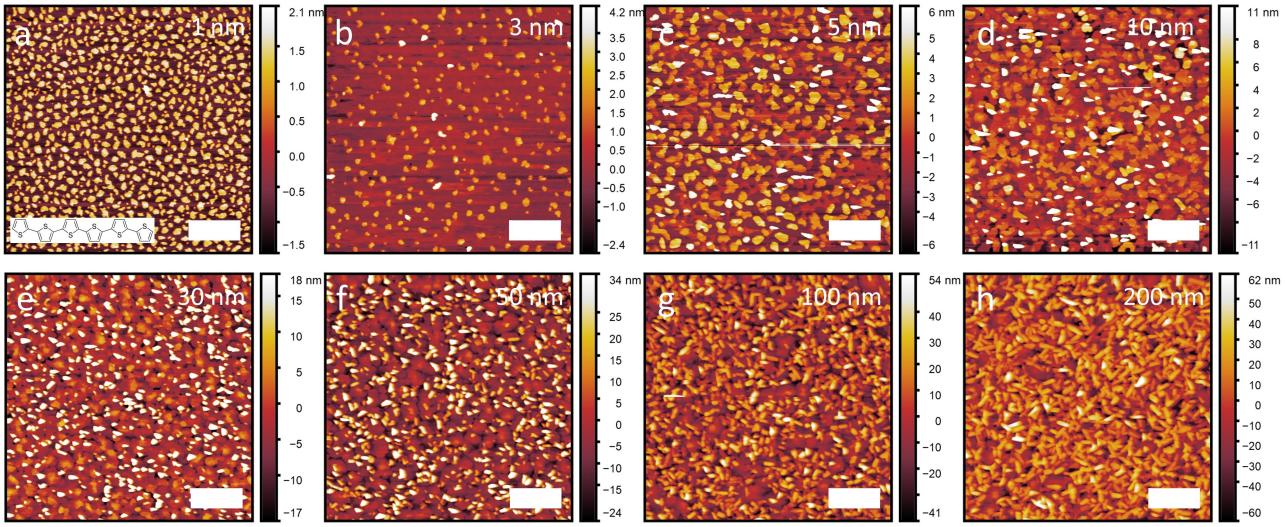

Figure S8: Atomic force microscope scans of α-6T deposited at a rate of 0.1 Å/s on a Si/SiO_2 substrate heated to 80 °C. Layer thickness is given in the top-right corner of each image. Scale bar is 1 μm.

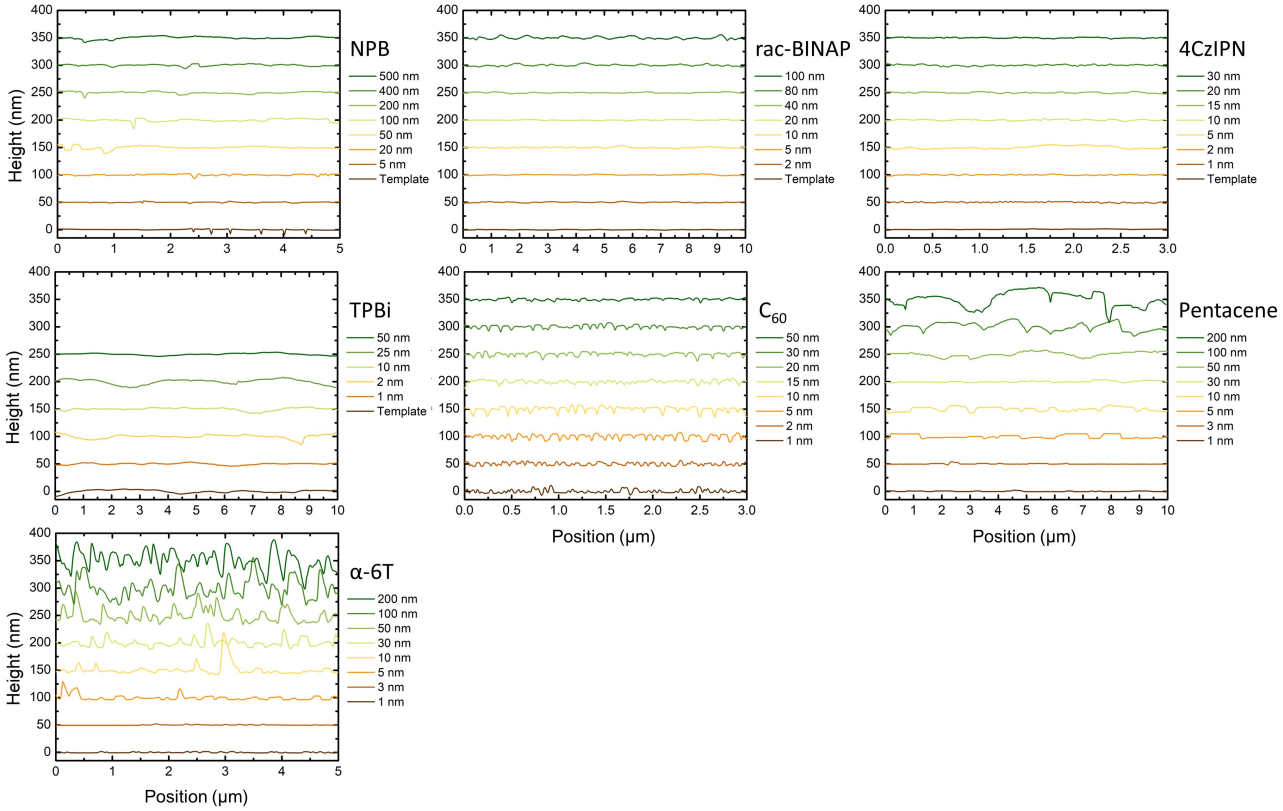

Figure S9: Horizontal line profiles taken at the midpoint of each AFM scan in Fig. S2-S8. Note the change in roughness for pentacene and α-6T is significantly larger than for the other five (low aspect ratio) materials.

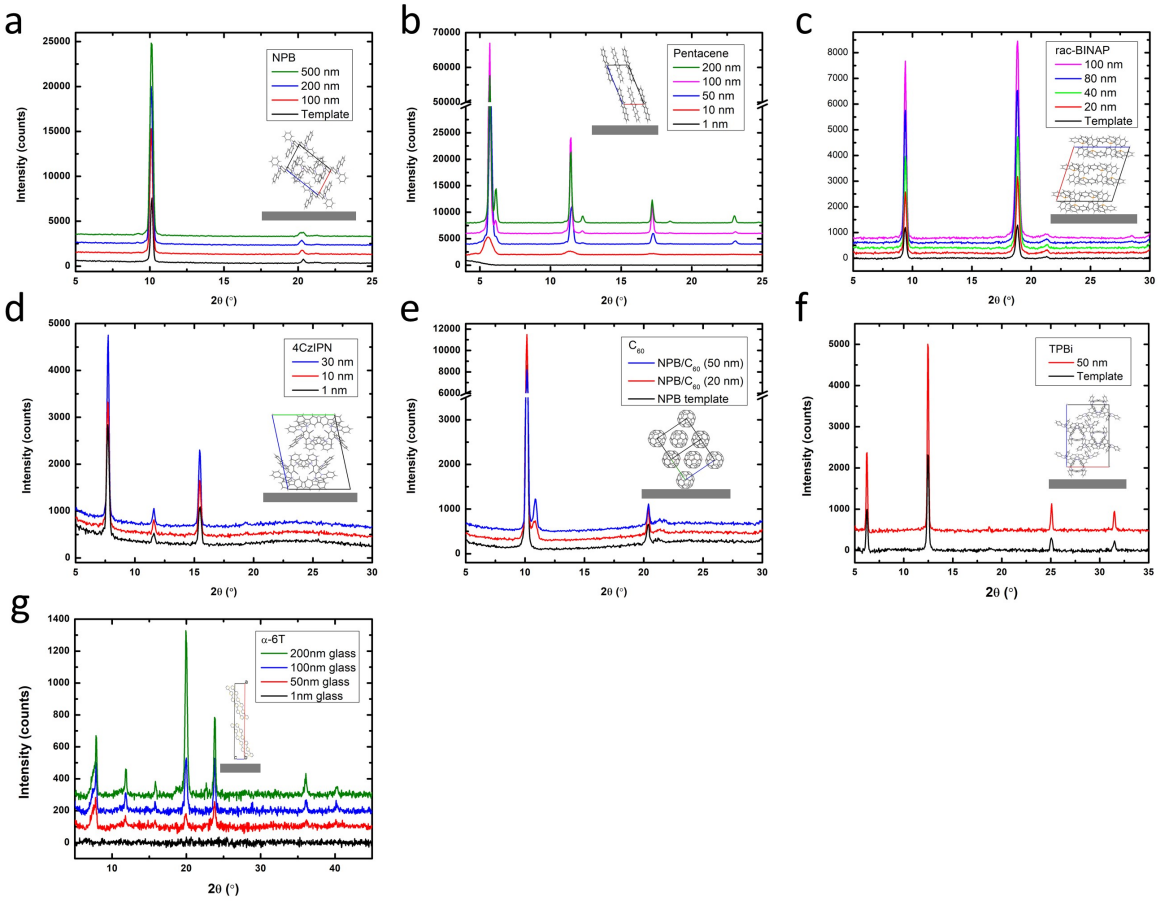

Figure S10: X-ray diffraction data of the material systems studied in this work. Scans were taken at various thicknesses showing that the peak intensity increases as thickness increases. This indicates the highly crystalline nature of these films and that depositing additional material on the template layer, or SiO_2 in the case of pentacene and α-6T, propagates the crystal growth. In the case of pentacene we see a second crystal phase emerge starting at about 50 nm of growth. The two phases are from the substrate induced thin-film phase and the bulk triclinic phase.[7] Inset shows the side-on view of the molecular packing for each crystal with respect to the substrate.

Table S2: Out-of-plane crystal orientation determined by XRD for the materials in Fig. S10 along with their respective Cambridge Structural Database (CSD) entry codes. For C_{60}, the Inorganic Crystal Structure Database entry number is given. For the materials studied with molecular dynamic simulations, these are the orientations used.

Material	Out-of-plane (hkl)	CSD Entry
NPB	(101)	REHJAQ
Pentacene	(001)	PENCEN
rac-BINAP	(100)	XAZGUC
4CzIPN	(001)	YUGDOV
C_{60}	(111)	74523
TPBi	(001)	JUXSUT01
α-6T	(100)	ZAQZUM

Molecular dynamic simulations

Simulation details

For simple ad-molecule surface simulations, we placed one ad-molecule on top of the island terrace and simulated its motion over the terrace under NVT canonical ensemble (constant number of particles, volume and temperature) at 300 K for at least 10 ns. In steered-molecular dyanamics (SMD) simulations, we attached an artificial spring to the ad-molecule and pulled it towards a pre-defined destination. The SMD code within LAMMPS then integrates the force to calculate the free energy with respect to the reaction coordinate (i.e. the distance travelled). Before we begin to pull the ad-molecule in SMD, we ran two separate simulations in which the ad-molecule was either on top of the island or at the side of the island. For these preliminary studies we used the NVE microcanonical ensemble (constant number of particle, volume and total energy) for 1 ns to determine an appropriate starting position for the ad-molecule on the terrace and the final destination of the ad-molecule after the descent, respectively. We broke down the step-edge descent process into two steps: Firstly, we pulled the ad-molecule horizontally across the island and stopped at a local free energy minimum when the ad-molecule was very near to the step-edge (approximately 5 Å away from the step-edge); we then pulled the ad-molecule to the final destination at

the side of the island which we predetermined from the NVE simulation. The process is illustrated in S11a. In all the SMD simulations, we used an NVT ensemble at 300 K. From the diffusion simulation, we calculate the mean squared displacement (MSD) of the traces using multi-time origins as defined in the usual way by Eq. 1

$$MSD =< \frac{1}{N} \sum_{i}^{N} |r(t) - r(t_0)|^2 > \tag{1}$$

where $N = 1$ for a single ad-molecule, $r(t)$ is the coordinate of the center of the mass of the ad-molecule at time, t, and t_0 is the time origin. We used a "sliding window" approach[8] to calculate the MSD over all the possible time origins with lag time τ, where τ is less than the length of the simulation time.

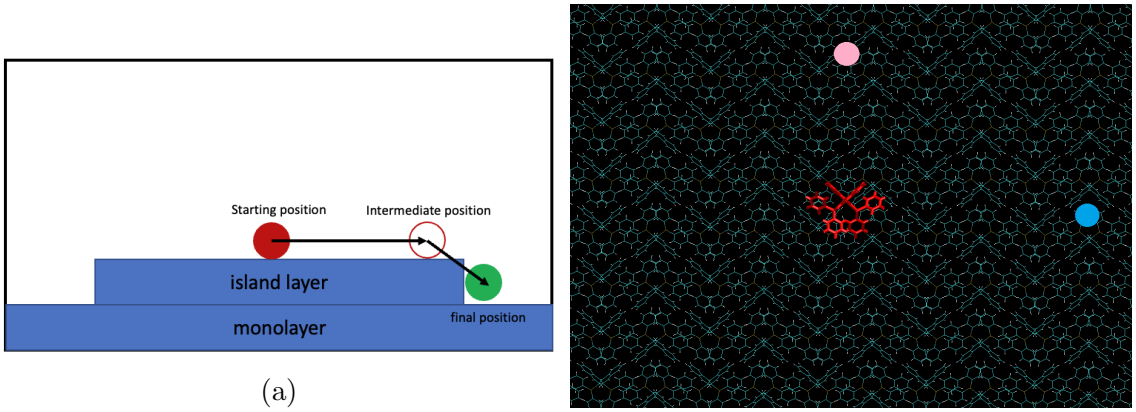

(a) (b)

Figure S11: (a) An illustration of the steered molecular dynamics simulation procedure. The red sphere represents the starting position of the ad-molecule on top of the island and the green sphere is the final position of the ad-molecule at the side of the island after the step-edge descent. The open red circle represents the intermediate position at a local free energy minimum during the horizontal pulling of the ad-molecule. The underlying monolayer and the island layer are shown as blue shaded rectangles and the external black lines represent the periodic boundaries of the simulation box. (b) A top view of the rac-BINAP terrace and the two directions in which we pulled the ad-molecule. The red molecule indicates the ad-molecule, the pink circle indicates the [010] direction and the blue circle indicates the [001] direction.

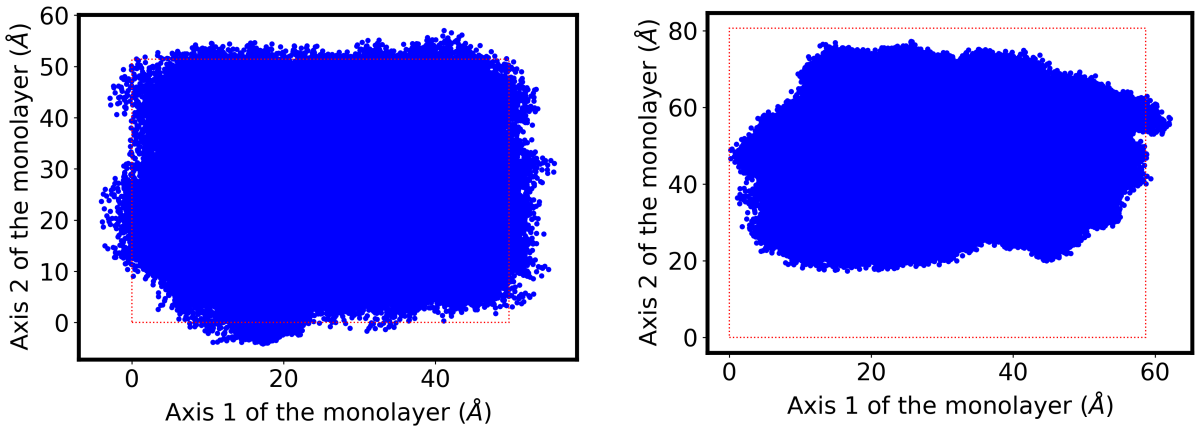

(a) α-6t

(b) rac-BINAP

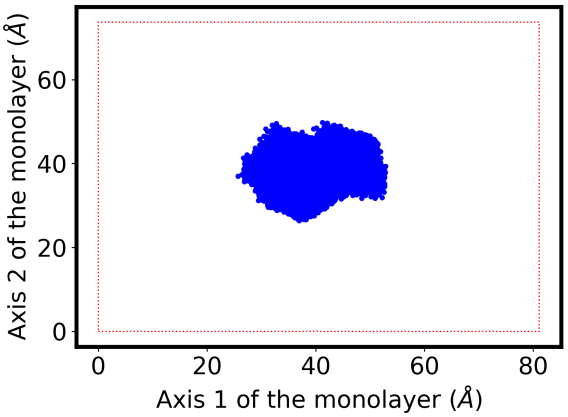

(c) NPB

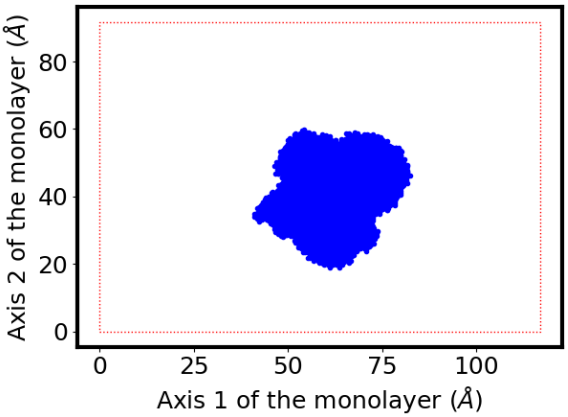

(d) TPBi

Figure S12: Two dimensional trace of the ad-molecule on the monolayer while preserving the 2D geometry information. Each atom within the ad-molecule is plotted as a dot on the graph and the red dashed line represents the boundary of the monolayer.

Effects of aggregation on mobility and $E_{\mathbf{ES}}$

Previous works have studied how aggregation of high aspect ratio molecules can affect the growth process.[9–11] Therefore, we simulate aggregated α-6T molecules to investigate its role in molecular mobility and the step-edge descent process. First, simulations are initialized with 2, 5, 10 and 50 α-6T molecules on a thin-film surface. We use a 2D monolayer of 150x160 Å^2 to accommodate the additional ad-molecules and run each simulation for 10 ns. We acknowledge that the experimental deposition rate may not result with this many molecules laying perfectly flat on the surface. However, the goal is to analyze how the for-

mation of aggregates affect the mobility of the ad-molecules. The mean square displacement (MSD) curve of each system is shown in Fig. 5e. The general trend is that the mobility decreases as the number of ad-molecules increase from 2 to 50. The α-6T aggregates are essentially immobile when there are 10 or 50 ad-molecules on the surface. For 2 ad-molecules, if their initial positions are close (i.e. 25 Å apart), they will immediately aggregate. If their initial distance is large, 130 Å apart for example, both molecules diffuse in-plane prior to aggregating, as manifested by the drop in MSD after 4 ns in Fig. 5e. We extended the simulation of 2 ad-molecules on a small island layer (around 90 Åin width) to 50 ns and on large island layer (around 160 Åin width) to 20 ns. Contrary to the surface diffusion simulation of single α-6T molecules, spontaneous step-edge descent does not occur when aggregates are formed in both sizes of the monolayer. We also examine how aggregation affects the E_{ES} during SMD simulations. We place two molecules at the center of an island layer and pull only on the one closest to the step-edge. For rac-BINAP, we only performed this in the preferred [010] direction. In every system, the two ad-molecules move together despite only one molecule being pulled. For α-6T, the remaining ad-molecule spontaneously descends over the edge after the first molecule descends, which is consistent with the previous conclusion that the E_{ES} of single α-6T is low. However, such spontaneous descent does not happen for molecules with low AR. We record the energy barrier in Tab. S6. In all four systems, the E_{ES} increases compared to the previous SMD simulations where only a single molecule on the thin-film surface was studied. However, the extra energy barrier due to aggregation is most significant for α-6T. If we define the extra E_{ES} from the aggregation as $E_{2mols} - 2 * E_{1mol}$, then α-6T aggregates experience an energy barrier 13 times higher than a single ad-molecule, sharply reducing the likelihood of spontaneous step-edge descent. The energy barrier seen by a rac-BINAP or TPBi aggregates is roughly 2-3 times that experienced by a single molecule, while for NPB the energy difference experience by a single molecule versus as aggregate is negligible.

Table S3: Free energy barriers to dissociate from a step-edge for α-6T, rac-BINAP (in the [010] direction), NPB and TPBi.

system	E_{edge} (kcal/mol)
α-6T	between -1.4 and -0.6
rac-BINAP [010]	5.6
NPB	7.7
TPBi	15.2

Table S4: Slopes of the lines fit to the MSD data in Fig. 4d (diffusion on an island) and Fig. 4e (diffusion on a monolayer).

system	D_{island} (cm^2/ns)	$D_{\text{monolayer}}$ (cm^2/ns)
α-6T	6.10E-06	5.26E-04
rac-BINAP	2.72E-06	3.57E-05
NPB	5.13E-08	5.61E-06
TPBi	9.91E-07	2.11E-05

Table S5: Slopes of the lines fit to the MSD data in Fig. S13 (diffusion of α-6T aggregation)

system	$D_{\text{aggregation}}$ (cm^2/ns)
2 molecules, 130 Å apart initially	9.13E-05
2 molecules, 25 Å apart initially	2.33E-05
5 molecules, 25 Å apart initially	2.17E-05
10 molecules	1.20E-06
50 molecules	1.64E-06

Table S6: Free energy barriers to step-edge descent for two aggregated ad-molecules. Energy barrier, E_1, is experienced during the horizontal pulling over the terrace and E_2 is the energy barrier of the descent from the island. The additional energy needed to descend is $E_{diff} = E_2 - E_1$. All energies are given in kcal/mol.

system	E_1	E_2	E_{diff}
α-6T	0.8	7.7	6.9
rac-BINAP [010]	6.9	12.2	5.3
NPB	8.7	14.3	5.6
TPBi	16.4	33.2	16.7

References

(1) Liscio, F.; Albonetti, C.; Broch, K.; Shehu, A.; Quiroga, S. D.; Ferlauto, L.; Frank, C.; Kowarik, S.; Nervo, R.; Gerlach, A. et al. Molecular Reorganization in Organic Field-Effect Transistors and Its Effect on Two-Dimensional Charge Transport Pathways. *ACS*

Nano **2013**, *7*, 1257–1264.

(2) Liscio, F.; Milita, S.; Albonetti, C.; D'Angelo, P.; Guagliardi, A.; Masciocchi, N.; Valle, R. G. D.; Venuti, E.; Brillante, A.; Biscarini, F. Structure and Morphology of PDI8-CN2 for n-Type Thin-Film Transistors. *Advanced Functional Materials* **2012**, *22*, 943–953.

(3) Hlawacek, G.; Puschnig, P.; Frank, P.; Winkler, A.; Ambrosch-Draxl, C.; Teichert, C. Characterization of step-edge barriers in organic thin-film growth. *Science* **2008**, *321*, 108–111.

(4) Dürr, A. C.; Schreiber, F.; Ritley, K. A.; Kruppa, V.; Krug, J.; Dosch, H.; Struth, B. Rapid Roughening in Thin Film Growth of an Organic Semiconductor (Diindenoperylene). *Physical Review Letters* **2003**, *90*, 016104.

(5) Yim, S.; Jones, T. S. Anomalous scaling behavior and surface roughening in molecular thin-film deposition. *Physical Review B* **2006**, *73*, 161305.

(6) Dull, J. T.; Wang, Y.; Johnson, H.; Shayegan, K.; Shapiro, E.; Priestley, R. D.; Geerts, Y. H.; Rand, B. P. Thermal Properties, Molecular Structure, and Thin-Film Organic Semiconductor Crystallization. *The Journal of Physical Chemistry C* **2020**, *124*, 27213–27221.

(7) Cheng, H. L.; Mai, Y. S.; Chou, W. Y.; Chang, L. R.; Liang, X. W. Thickness-dependent structural evolutions and growth models in relation to carrier transport properties in polycrystalline pentacene thin films. *Advanced Functional Materials* **2007**, *17*, 3639–3649.

(8) Maginn, E. J.; Messerly, R. A.; Carlson, D. J.; Roe, D. R.; Elliot, J. R. Best practices for computing transport properties 1. Self-diffusivity and viscosity from equilibrium molecular dynamics [article v1. 0]. *Living Journal of Computational Molecular Science* **2019**, *1*, 6324–6324.

(9) Roscioni, O. M.; D'Avino, G.; Muccioli, L.; Zannoni, C. Pentacene Crystal Growth on Silica and Layer-Dependent Step-Edge Barrier from Atomistic Simulations. *Journal of Physical Chemistry Letters* **2018**, *9*, 6900–6906.

(10) Zorba, S.; Shapir, Y.; Gao, Y. Fractal-mound growth of pentacene thin films. *Physical Review B* **2006**, *74*.

(11) Ruiz, R.; Choudhary, D.; Nickel, B.; Toccoli, T.; Chang, K. C.; Mayer, A. C.; Clancy, P.; Blakely, J. M.; Headrick, R. L.; Iannotta, S. et al. Pentacene thin film growth. *Chemistry of Materials* **2004**, *16*, 4497–4508.